Hindawi
Mathematical Problems in Engineering
Volume 2020, Article ID 7319871, 9 pages
https://doi.org/10.1155/2020/7319871

Research Article

Calculation of Unloading Area of Internal Gear Pump and Optimization

Shanxin Guo and Dagui Chen

Smart Home Information Collection and Processing on Internet of Things Laboratory of Digital Fujian, Fujian Jiangxia University, Fuzhou 350108, China

Correspondence should be addressed to Shanxin Guo; guosx510@fjjxu.edu.cn

Received 2 April 2020; Revised 17 July 2020; Accepted 24 July 2020; Published 26 August 2020

Academic Editor: Xiao-Qiao He

In order to obtain the calculation method of the unloading area of the internal gear pump during oil trapping, a pair of internal gears including an external gear and an internal gear was used as the research object to simulate the oil trapping process. The geometric relationship during the meshing process was established, and the unloading area expression was obtained by using the geometric pattern expansion method with the variable f as the independent variable. Guided by a mathematical model, two improved optimization schemes were proposed for the internal gear tooth profile, and the unloading area expressions s_{ud}, s_{uda}, and s_{udb} were obtained. Taking the meshing gear pair with module 3 and number of teeth 13/19 as examples, the simulation results were very consistent with the existing literature. The reliability of the model and the feasibility of the optimization scheme are obtained based on the theoretical analysis and calculation results. This calculation method of unloading area can be applied to the same type of gear pump design in the future, providing a reference for the design of high pressure and low noise gear pumps.

1. Introduction

The internal gear pump has oil trapping phenomenon during the rotating work and has smaller oil trapping changes than the external gearing [1]. At present, gear pump oil trapping phenomenon is one of the key factors restricting higher performance [2]. In order to improve the design performance of the gear pump, Erturk et al. analyzed the oil trap mechanism of the hydraulic pump and found its variation rule and found that the backlash of the gear pair can affect the oil trap [3]. Sun et al. proposed the definition of backlash unloading of gear pumps and compared and verified the results [4]. In order to further reduce the trapped oil, Li and Liu calculated the unloading area of the gear pump and then performed a simulation analysis [5]. Zang et al. proposed a new method for reducing the trapped oil pressure of the gear pump [6]. Above those was an external gear pump. Tt is still a large difference in the structure between the internal gear and the external gear pump. There is less research on oil trapping and unloading of the internal gear pump. On internal gear pumps, Yanada et al. had studied the phenomenon of oil trapping between gear pairs and pointed out the source of the oil trap [7]. Zhou et al. had adopted a discrete method to study conjugate gears and obtained the oil trap of this pump [8, 9]. Song et al. designed the conjugated straight-line internal gear pairs for fluid power gear machines and got the unloading curve graphically by a discretization approach [10]. Above all, research methods are of reference to internal gear pumps with involute tooth profiles, but they are not continuous in calculation and not completely accurate. In these references, the unloading area was obtained by the graphic method, and the change law of the area size with processing and parameters was analyzed, but the results of such processing have limitations. Therefore, this paper will overcome the shortcomings mentioned above and, then, use calculation and derivation methods to obtain accurate results of unloading area. The conclusions obtained can provide theoretical guidance for the model parameters and design principles of the internal gear pump and can also optimize the unloading area according to the processing and forming methods.

2. Oil Trapping Process Description and Calculation Basis of Internal Gear Pump

2.1. Description of Oil Trapped Process. A pair of backlash-free gear tooth rotation processes are used as an analysis to explain the oil trapping and unloading of the internal gear pump. In this process, the unloading groove can be designed. Although its design is more flexible and has more geometric forms, its design principles are basically the same [11]. Figure 1 shows oil trapping and unloading process of internal gear pump, the external gear O_1, and the internal gear O_2 from an oil trapped area. This article uses them as an example to explain that they pass through the boundary *ud* of the rectangular unloading groove [12]. p, n_1, and n_0 are gear joint nodes, meshing points, and backlash points. The meshing point n_1 is moving along the meshing line during the rotation of the gear pair. Figure 1(a) shows the minimum oil trapped area, Figure 1(b) shows *ud* on the involute of gear O_1 and involute of gear O_2, Figure 1(c) shows *ud* on the top circle of gear and gear O_2 transition curve, Figure 1(d) shows *ud* on the tooth top circle of gear O_1 and the tooth root circle of gear O_2, Figure 1(e) shows *ud* on tooth top circle of gear O_1 and gear O_2 the transition curve, Figure 1(f) shows *ud* involute of gear O_1 and gear O_2 transition curve, and Figure 1(g) shows *ud* on the involute of gear O_1 and gear O_2.

The length from point p to point n_1 is f. The length of f in Figure 1(a) is f_0, and $f_0 = P_b/4$. When f changes to the position of Figure 1(g) as n_1 moves, f is f_g, $f_g = r_{b,1}(\tan\alpha_{\alpha,1} - \tan\alpha')$. When point p moves to *ud* along the meshing line of the gear pair, the length of f at this time is f_a and $f_a = B_{ud}/\cos\alpha'$. The above equations p_b, $r_{b,1}$, $\alpha_{\alpha,1}$, α', and B_{ud} are the base pitch of the gear O_1, the base circle radius, the pressure angle of the tooth top circle, the meshing angle, and the distance from *ud* to the line connecting the center of gear O_1 and gear O_2.

2.2. Mathematical Knowledge. Figure 2 is an outline of an internal gear processed by a forming method. With the center of the circle O_2 as the origin of the coordinates and the symmetry line of a cogging as the y-axis, a rectangular coordinate system xO_2y is established. This coordinate system can be rotated around point O_2 with a rotation angle of θ. The t_1t_2 line segment is an involute equation, and the r_1r_2 line segment is a transition curve. Point t can slide on the line segment t_1t_2 arbitrarily, and the direction is to move from point t_1 to point t_2. Point r can slide on the line segment r_1r_2 arbitrarily, and the direction is to move from point r_1 to point r_2. Suppose α_x, r_x, x_x, y_x, and θ_x are the gear pressure angle at point x, the corresponding radius, the abscissa in the coordinate system, the ordinate in the coordinate system, and the rotation angle $\angle t_1o_2t = \varnothing$, $\angle r_1o_2t = \zeta$. By the definition of the involute function, any two points on the involute line can be connected to the center of the circle to form a sector [13]:

$$\begin{cases} \varnothing = (\tan\propto_t - \propto_t) - (\tan\propto_{t1} - \propto_{t1}), \\ S_{inv} = \int \dfrac{r_t^2(\phi)}{2} d\phi. \end{cases} \tag{1}$$

Let the fan-shaped area enclosed by the line segment t_1t_2 and the radius of point t_1 and point t_2 be expressed as $S_{\text{inv}}\Big|_{t1}^{t2}$, which can be deduced from (1), $S_{\text{inv}}|_{t1}^{t2} = \int((r_t^2(\varnothing))/2)d\varnothing = (r_{b,1}^2/2)\int_{\alpha_{t1}}^{\alpha_{t2}}(\sec^4\alpha_t - \sec^2\alpha_t)d\propto_t = r_{b,1}^2((\tan^3_{\alpha_{t2}} - \tan^3_{\alpha_{t1}})/6)$.

In rectangular coordinate system, $\zeta = \tan^{-1}(x_r/y_r) - \tan^{-1}(x_{r1}/y_{r1})$. Suppose that the fan-shaped area enclosed by the contour of the line segment r_1r_2 and the radius of point r_1 and point r_2 can be expressed as $S_{\text{sta}}|_{r1}^{r2}$. According to [14], $S_{\text{sta}} = \Big|_{r1}^{r2}(r'^2/6)(\theta_{r2}^3 - \theta_{r1}^3) - (mh_{a0}^*/2)(r' - mh_{a0}^*)(\theta_{r2} - \theta_{r1})$ the above formula, h_{a0}^* and m are the tooth height coefficient and modulus of the rack cutter for processing the gear profile and r' is the pitch circle radius.

The gears produced by the envelope method have regular geometric outer contours [15]. Figure 3(a) shows the outline of an external gear machined by generating method, and Figure 3(b) shows the profile of an internal gear machined by generating method. Let $r_{a,1}$, $r_{a,2}$, $r_{f,1}$, $r_{f,2}$ be the radius of the top circle and root circle of the external gear and internal gear. Let $\angle a_1o_1a_2 = \sigma$, $\angle a_5o_1a_6 = \tau$, $\angle c_1o_2c_4 = \mu$, $\angle c_2o_1c_3 = \lambda$, $\angle c_5o_1c_6 = \omega$, and the corresponding sector areas are S_{top2}, S_{root1}. Then, $S_{\text{top2}} = 0.5r_{a,1}^2\sigma$, $S_{\text{root1}} = 0.5r_{f,1}^2\tau$. Once the gear parameters are determined, the radius of the root and top circles of the gear and the angle between each gear tooth can be determined [16]; then, S_{top1} and S_{root1} are fixed values. Similarly, the sector areas corresponding to the top and root circles of the internal gear are S_{top2} and S_{root2}. Then, $S_{\text{top2}} = 0.5r_{a,2}^2\lambda$ and $S_{\text{root1}} = 0.5r_{f,2}^2\omega$.

3. Establishing the Calculation Model of Unloading Area

3.1. Mathematical Model. Figure 4(a) is a pair of internal gear pairs and e is the center distance. The Cartesian coordinate systems $x_1O_1y_1$ and $x_2O_2y_2$ are established by using the gear circle centers O_1 and O_2 as the coordinate origins and the symmetry lines of the external gear teeth and internal gear grooves as the y-axis. Taking Figure 1(a) as the initial position, the rotation angles of O_1 and O_2 are θ_1 and θ_2, respectively. During the rotation, the outline of the external gear, the profile of the internal gear, and *ud* intersect at points w and v, respectively. Among them, $S_{\cap wo1n1}$ and $S_{\cap vo2n1}$ are the radius of point w, point n_1, point v, and the area enclosed by the contour line of the gear, respectively. For ease of calculation, let $S_1 = S_{\cap vo2n1}$, $S_2 = S_{\Delta o2vn1}$, $S_3 = S_{\Delta wvn1}$, $S_4 = S_{\cap wo1n1}$, and $S_5 = S_{\Delta o1\omega n1}$. Then, fold O_2v and O_2n_1 along vn_1 to get Figure 4(b). According to the graph, the unloading area S_{ud} can be expressed as

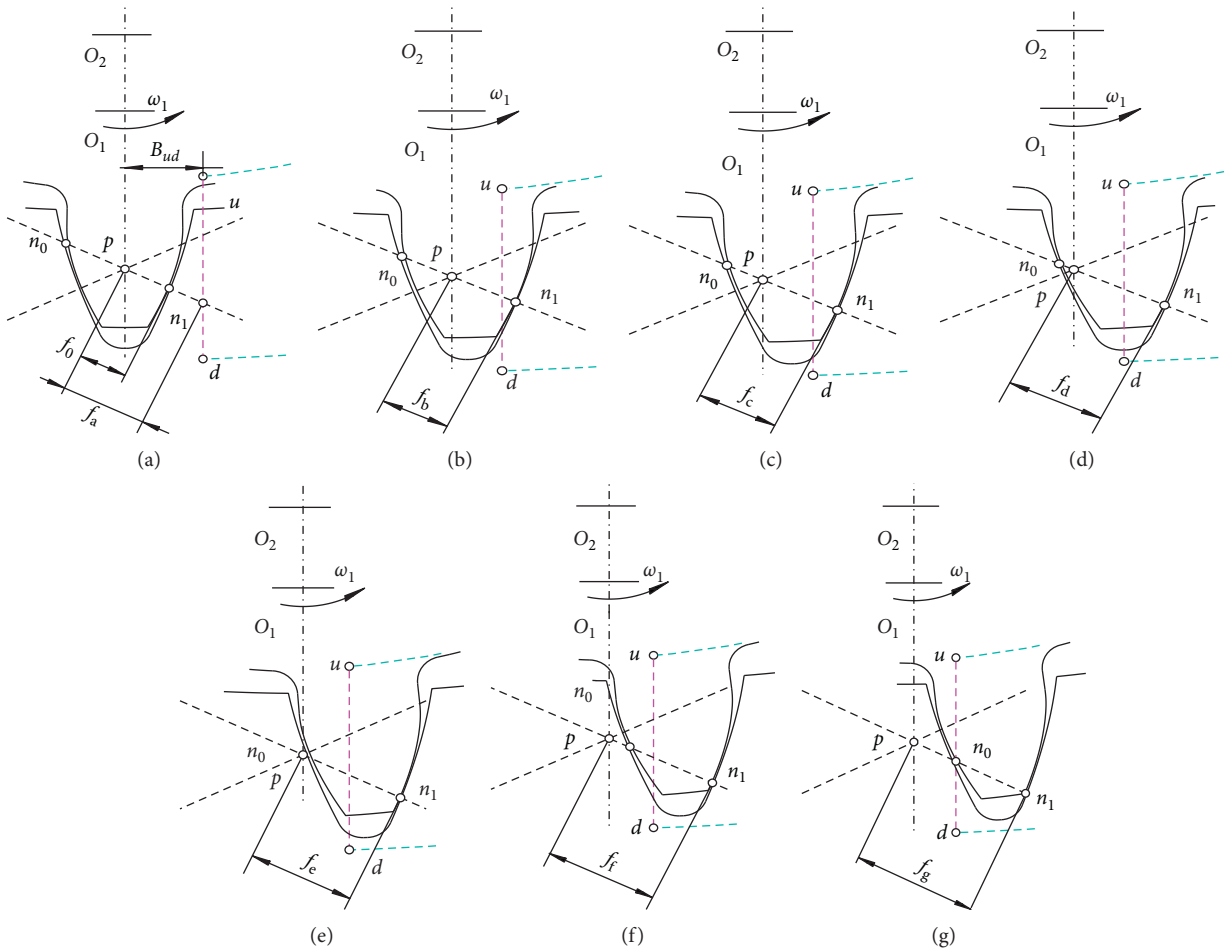

Figure 1: Oil trapping and unloading process of internal gear pump.

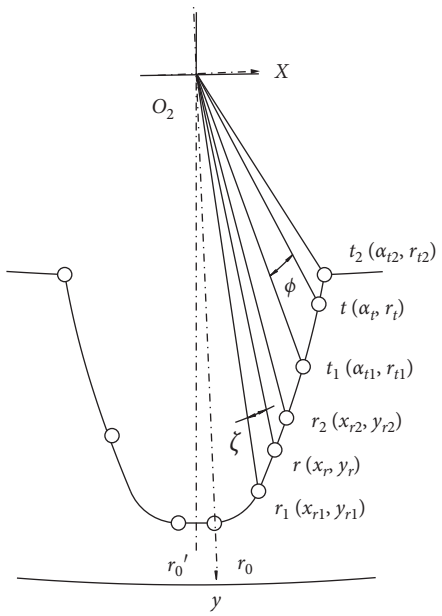

Figure 2: Internal gear profile.

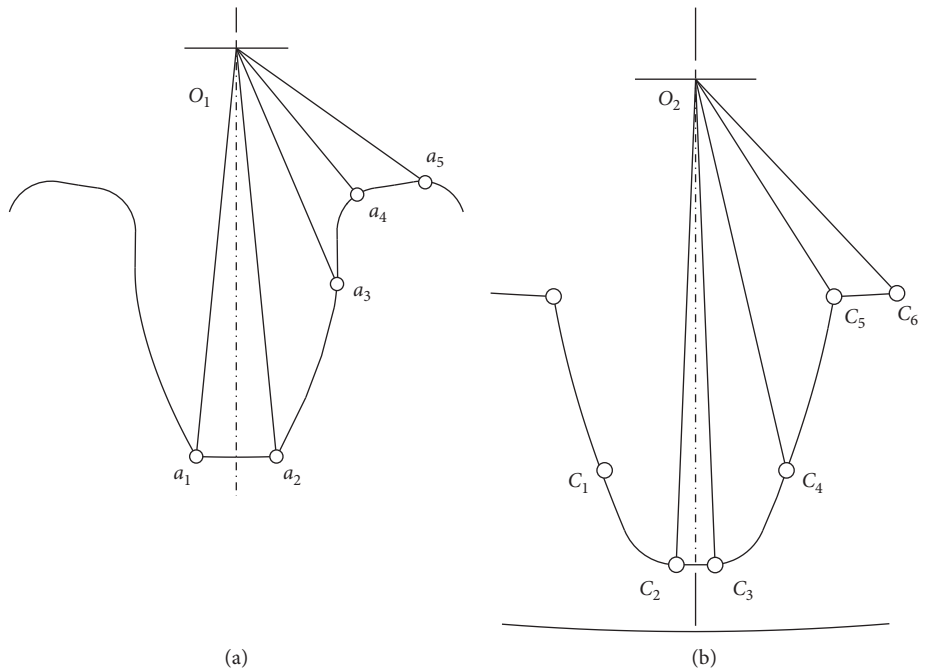

Figure 3: Gear profile machined by unrolling.

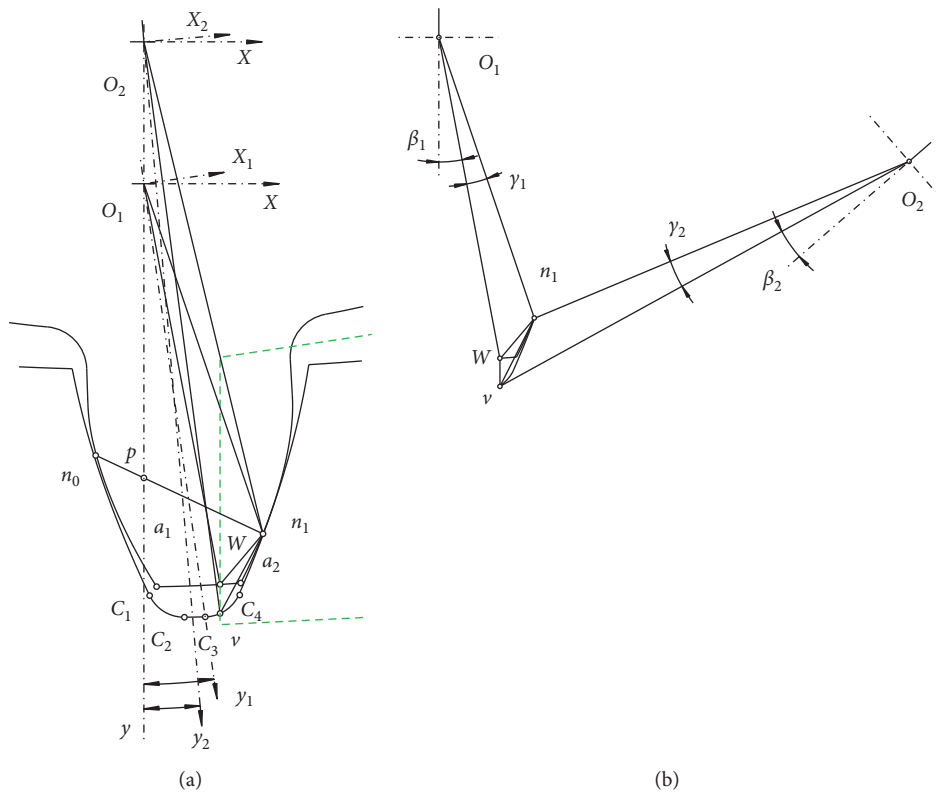

Figure 4: A pair of internal gears meshing.

$$S_{\mathrm{ud}} = S_1 - S_2 + S_3 - (S_4 - S_5). \tag{2}$$

Let $\angle po_1w = \beta_1$, $\angle n_1o_1w = \gamma_1$, $\angle po_2v = \beta_2$, $\angle n_1o_2v = \gamma_2$. $r_{p,1}$, $r_{p,2}$, $r_{n1,1}$, $r_{n1,2}$ are the pitch circle radius and the meshing point radius of O_1 and O_2, respectively. l_{vn1}, l_{wn1}, and l_{vw} are distances between points v, w, and n_1. From the geometric relationship in the figure,

$$\begin{cases} r_{n1,1}^2 = r_{p,1}^2 + f^2 - 2r_{p,1}f\cos\left(\dfrac{\pi}{2} + \alpha'\right), \\ l_{wn1}^2 = r_{n1,1}^2 + r_w^2 - 2r_{n1,1}r_w\cos\beta_1, \\ r_{n1,2}^2 = r_{p,2}^2 + f^2 - 2r_{p,2}f\cos\left(\dfrac{\pi}{2} + \alpha'\right), \\ l_{vn1} = r_{p,2}^2 + f^2 - 2r_{p,2}f\cos\left(\dfrac{\pi}{2} + \alpha'\right), \\ l_{vw} = r_w\cos\gamma_2 - r_v\cos\gamma_1 - e. \end{cases} \tag{3}$$

Let

$$\begin{cases} \rho_1 = \dfrac{\left(r_w + r_{n1,1} + l_{wn1}\right)}{2}, \\ \rho_2 = \dfrac{\left(r_v + r_{n1,2} + l_{vn1}\right)}{2}, \\ \rho_3 = \dfrac{(l_{wn1} + l_{vn1} + l_{wv})}{2}. \end{cases} \tag{4}$$

From Heron's formula,

$$\begin{cases} S_2 = \left[\rho_2(\rho_2 - r_v)\left(\rho_2 - r_{n1,2}\right)(\rho_2 - l_{vn1})\right]^{1/2}, \\ S_3 = \left[\rho_3(\rho_3 - l_{wn1})(\rho_3 - l_{wv})(\rho_3 - l_{vn1})\right]^{1/2}, \\ S_5 = \left[\rho_1(\rho_1 - r_w)\left(\rho_1 - r_{n1,1}\right)(\rho_1 - l_{wn1})\right]^{1/2}. \end{cases} \tag{5}$$

Apply sine theorem in Δwo_1n_1, Δvo_2n_1:

$$\begin{cases} \dfrac{f}{\sin(\beta_1 + \gamma_1)} = \dfrac{r_{p,1}}{\sin\left[\pi - \beta_1 - \gamma_1 - ((\pi/2) + \alpha')\right]}, \\ \dfrac{f}{\sin(\beta_2 + \gamma_2)} = \dfrac{r_{p,2}}{\sin\left[\pi - \beta_2 - \gamma_2 - ((\pi/2) + \alpha')\right]}. \end{cases} \tag{6}$$

Deduce

$$\begin{cases} \gamma_1 = \tan^{-1}\dfrac{f\cos\alpha'}{r_{p,1} + f\sin\alpha'} - \beta_1, \\ \gamma_2 = \tan^{-1}\dfrac{f\cos\alpha'}{r_{p,2} + f\sin\alpha'} - \beta_2. \end{cases} \tag{7}$$

Since θ_1, θ_2, and f are linear functions, then from (2)–(7), only the changes of r_w and β_1 with θ_1, r_v and β_2 with θ_2 can be used to obtain the change of S_{ud}.

3.2. External Gear Rotation Parameters. When a_1 and a_2 are located on ud, β_1 can be expressed as $\beta_{1,a1} = \beta_{1,a2} = \sin^{-1}(B_{\mathrm{ud}}/r_{a,1})$. When points n_0, a_1, a_2, and n_1 are located on ud, these rotation angles θ_1 can be expressed as $\theta_{1,a} = (f_a - f_0)/r_{b,1}$, $\theta_{1,a1} = \beta_{1,a1} - (\sigma/2)$, $\theta_{1,a2} = \beta_{1,a2} + (\sigma/2)$, $\theta_{1,g} = (f_g - f_0)/r_{b,1}$. According to the structure of the external gear, when the point w moves to n_0a_1, a_2n_1 involute segment, according to the backlash-free meshing equation [17] and Figure 3(a), it can be obtained that

$$\begin{cases} \left|\theta_1 - \beta_1\right| = \dfrac{\pi + 4k_1\tan\alpha}{2z_1} - (\mathrm{inv}\alpha_w - \mathrm{inv}\alpha), \\ \sin\beta_1 = \dfrac{\left(B_{\mathrm{ud}}/r_{b,1}\right)}{\cos\alpha_w}. \end{cases} \tag{8}$$

If $\theta_1 \geq \beta_1$, it means that the w point is on the n_0a_1 line segment. If $\theta_1 < \beta_1$, it means that the w point is on the a_2n_1 line segment.

When the point w is on the a_1a_2 line segment, $r_w = r_{a,1}$, $\beta = \sin^{-1}(B_{\mathrm{ud}}/r_{a,1})$.

3.3. Internal Gear Rotation Parameters. If c_1 and c_4 are located on ud, $\beta_2$can be expressed as $\beta_{2,c1} = \beta_{2,c4} = \sin^{-1}(B_{\mathrm{ud}}/r_{f,2})$.

When the rotation process of O_2, several special points n_0, c_1, c_2, c_3, c_4, n_1, is located on ud, the corresponding rotation angle θ_2 changes to,

$$\begin{aligned} \theta_{2,a} &= \frac{f_a - f_0}{r_{b,2}}, \\ \theta_{2,c4} &= \beta_{2,a4} - \frac{\mu}{2}, \\ \theta_{2,c3} &= \theta_{2,c4} + \lambda, \\ \theta_{2,c2} &= \theta_{2,c3} + (\mu - 2\lambda), \\ \theta_{2,c1} &= \theta_{2,c2} + \lambda, \\ \theta_{2,g} &= \frac{f_g - f_0}{r_{b,2}}. \end{aligned} \tag{9}$$

$\theta_{2,a} \longrightarrow \theta_{2,g}$ is represented, respectively, as the process from f to the end of θ_2 when $f_a \longrightarrow f_g$.

According to the internal gear structure, when the v point moves to the n_0c_1 and c_4n_1 involute segments, the backlash-free meshing equation is combined with Figure 3(a):

$$\begin{cases} \left|\theta_2 - \beta_2\right| = \dfrac{\pi - 4k_2 \tan\alpha}{2z_2} + \left(\text{inv}\alpha_v - \text{inv}\alpha\right), \\ \sin\beta_2 = \dfrac{\left(B_{u\,d}/r_{b,2}\right)}{\cos\alpha_v}. \end{cases} \tag{10}$$

If $\theta_2 \geq \beta_2$, it means that the v point is on the n_1c_4 segment. If $\theta_2 < \beta_2$, it means that the v point is on the c_1n_0 segment. When the v point is at the transition curve c_1c_2, c_3c_4, as shown in the figure:

$$\left|\theta_2 - \beta_2\right| = \angle y_2o_2c_3 + \angle c_3o_2v = \frac{\mu}{2} - \lambda + \tan^{-1}\frac{x_v}{y_v}. \tag{11}$$

If $\theta_2 \geq \beta_2$, it means that the v point is in the c_3c_4 segment. If $\theta_2 < \beta_2$, it means that the v point is in the c_1c_2 segment. (x_v, y_v) is the coordinate value of the v point in the coordinate system of the figure.

When the v point is at the root circle c_2c_3, $\beta_2 = \beta_{2,c2} = \beta_{2,c3}$, and $r_v = r_{f,2}$, where $r_{f,2}$ is the radius of the O_2 root circle. Therefore,

$$S_4 = \begin{cases} 0, & \left(\theta_1 \leq \theta_{1,a}\right), \\ S_{\text{inv}}\big|_{t1=n_1}^{t2=w}, & \left(\theta_{1,a} < \theta_1 \leq \theta_{1,a_2}\right), \\ S_{\text{inv1}} + \dfrac{\theta_1 - \theta_{1,a_1}}{\sigma}S_{\text{top1}}, & \left(\theta_{1,a_2} < \theta_1 \leq \theta_{1,a_1}\right), \\ S_{\text{inv1}} + S_{\text{top1}} + S_{\text{inv}}\big|_{t1=n_0}^{t2=w}, & \left(\theta_{1,a_1} < \theta_1 \leq \theta_{1,g}\right), \end{cases}$$

$$S_1 = \begin{cases} 0, & \left(\theta_2 \leq \theta_{2,a}\right), \\ S_{\text{inv}}\big|_{t1=n1}^{t2=v}, & \left(\theta_{2,a} < \theta_2 \leq \theta_{2,c_4}\right), \\ S_{\text{inv2}} + S_{\text{sta}}\big|_{r1=c_4}^{r2=v}, & \left(\theta_{2,c_4} < \theta_2 \leq \theta_{2,c_3}\right), \\ S_{\text{inv2}} + S_{\text{sta2}} + \dfrac{\theta_2 - \theta_{2,c_3}}{0.5\mu - \lambda}S_{\text{root2}}, & \left(\theta_{2,c_3} < \theta_2 \leq \theta_{2,c_2}\right), \\ S_{\text{inv2}} + S_{\text{sta2}} + S_{\text{root2}} + S_{\text{sta}}\big|_{r1=c_2}^{r2=v}, & \left(\theta_{2,c_2} < \theta_2 \leq \theta_{2,c_1}\right), \\ S_{\text{inv2}} + 2S_{\text{sta2}} + S_{\text{root2}} + S_{\text{inv}}\big|_{t1=n_0}^{t2=v}, & \left(\theta_{2,c_1} < \theta_1 \leq \theta_{2,g}\right). \end{cases} \tag{12}$$

4. Optimized Design

If the internal gear pair parameters and center distance are determined, then, S_2, S_3, and S_5 are determined. The design goal hopes to optimize and increase S_{ud}. According to the aforementioned calculation model of S_{ud}, it can be achieved by increasing S_1 or decreasing S_4. Considering the actual situation, S_1 is easier to implement, so two optimization schemes are proposed for machining the outer contour of the internal gear with a forming tool or mold. The first method is to increase the radius of the tooth root circle; the second method is to eliminate the cogging transition curve segment on the gear profile. The improvement method is shown in Figures 5(a) and 5(b). Let the radius of the root circle of Figure 5(a) be r_{fa}, and the corresponding sector area is $S_{\text{root2}a} = 0.5r_{\text{fa}}^2\lambda$. During the rotation, the sector enclosed by the radii v and n_1 and their contour is S_{1a}:

$$S_{1a} = \begin{cases} 0, & \left(\theta_2 \leq \theta_{2,a}\right), \\ S_{\text{inv}}\big|_{t1=n_1}^{t2=v}, & \left(\theta_{2,a} < \theta_2 \leq \theta_{2,e_4}\right), \\ S_{\text{inv2}} + S_{\text{sta}}\big|_{r1=v}^{r2=e_4}, & \left(\theta_{2,e_4} < \theta_2 \leq \theta_{2,e_3}\right), \\ S_{\text{inv2}} + S_{\text{sta2}} + \dfrac{\theta_2 - \theta_{2,e_3}}{0.5\mu - \lambda}S_{\text{root2}a}, & \left(\theta_{2,e_3} < \theta_2 \leq \theta_{2,e_2}\right), \\ S_{\text{inv2}} + S_{\text{sta2}} + S_{\text{root2a}} + S_{sta}\big|_{r1=v}^{r2=e_2}, & \left(\theta_{2,e_2} < \theta_2 \leq \theta_{2,e_1}\right), \\ S_{\text{inv2}} + 2S_{\text{sta2}} + S_{\text{root2a}} + S_{\text{inv}}\big|_{t1=v}^{t2=n_0}, & \left(\theta_{2,e_1} < \theta_1 \leq \theta_{2,g}\right). \end{cases} \tag{13}$$

The unloading area of the first scheme is S_{uda}. S_{1a} can be derived by replacing S_1 in (2), then, obtaining S_{uda}.

Let the radius of the root circle of Figure 5(b) be r_{fb}, and its corresponding sector area is $s_{\text{root2}b}$, $s_{\text{root2}b} = 0.5r_{\text{fb}}^2\lambda$. During its rotation, the radii of points v and n_1 and their corresponding contour lines are enclosed in a fan shape, and their area is s_{1b} :

$$s_{1b} = \begin{cases} 0, & \left(\theta_2 \leq \theta_{2,a}\right), \\ s_{\text{inv}}\big|_{t_1=n_1}^{t_2=v}, & \left(\theta_{2,a} < \theta_2 \leq \theta_{2,q_4}\right), \\ s_{\text{inv2}} + \dfrac{\theta_2 - \theta_{2,q_1}}{\lambda}s_{\text{root2}b}, & \left(\theta_{2,q_4} < \theta_2 \leq \theta_{2,q_1}\right), \\ s_{\text{inv2}} + s_{\text{root2}b} + s_{\text{inv}}\big|_{t1=v}^{t2=n_0}, & \left(\theta_{2,q_1} < \theta_2 \leq \theta_{2,g}\right). \end{cases} \tag{14}$$

The unloading area of the second scheme is S_{udb}. S_{udb} can be derived by replacing S_1 in (2) with S_{1b}.

5. Simulation

Taking the parameters of medium and high pressure internal gear pumps of Fuzhou University Hydraulic Parts Factory as an example, enveloping processing, the first optimization scheme, and the second optimization scheme, the parameters are shown in Table 1.

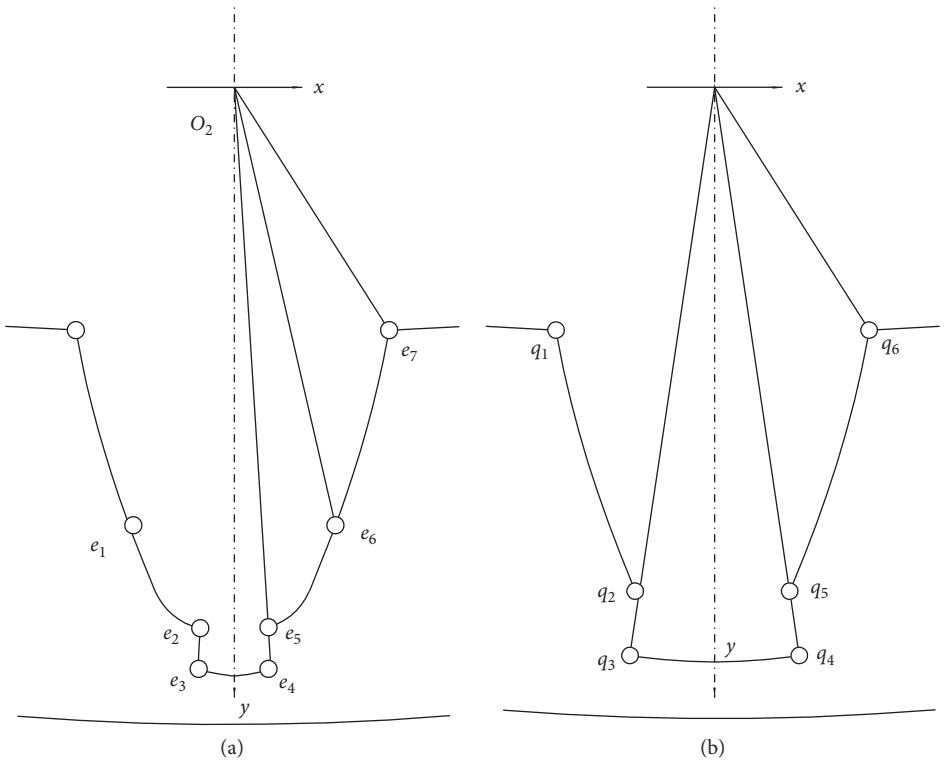

Figure 5: Optimizing the internal gear profile. (a) The first optimization scheme and (b) the second optimization scheme.

Table 1: Internal gear pump parameters.

Name of the parameter	Parameter	Value
Number of teeth	z_1/z_2	13/19
Modulus (mm)	m	3
Center distance (mm)	e	9.278
Pressure angle (°)	α	20
Coefficient of rack cutter tip height	h_{a0}^*	1.25
External gear profile shift coefficient	K_1	0.432
Internal gear profile shift coefficient	K_2	0.55
Unloading groove boundary distance (mm)	B_{ud}	2.035
The first solution root radius (mm)	r_{fa}	32.0
The second solution root radius (mm)	r_{fb}	33.80

During the gear rotation, the position variable f is left-right symmetric with the position shown in Figure 1(a). MATLAB software is used to draw the unloading area, which changes with f in a meshing cycle as shown in Figure 6.

The parameters provided in Table 1 are the original data of the gear pump during the actual design and manufacture, which are consistent with the parameters under the number of different teeth ($z_1 + z_2 = 32$) in [18]. From the results of the simulation of S_{ud} in Figure 6, the change law of S_{ud} is very consistent with [18] during a period in which the position variable f changes. This verifies the correctness of the calculation of the unloading area S_{ud}.

Once the gear parameters are determined, the outer contour of the gear teeth formed by the envelope method is a certain value. Therefore, the shaping method of the internal tooth contour machining method is improved.

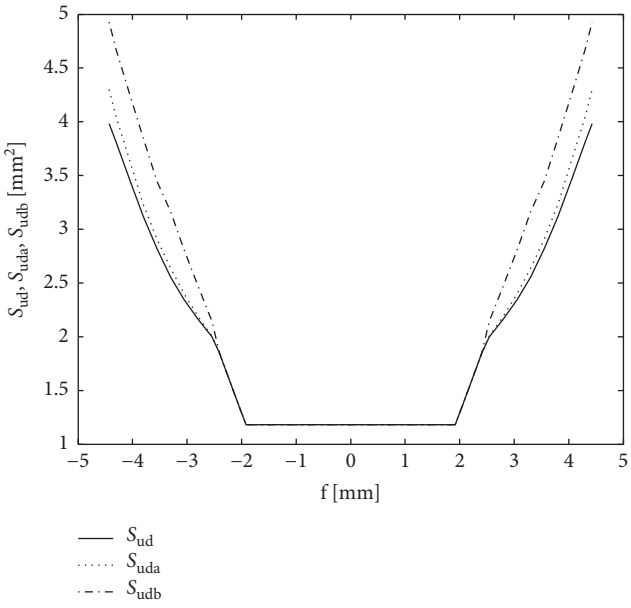

Figure 6: Changes in unloaded area.

From the changes of S_{uda} and S_{udb} in Figure 6, it can be seen that increasing the root circle radius of the internal gear tooth profile can obtain a larger unloading area S_{ud} during the oil trapping process. The larger the radius of the root circle, the larger S_{ud}. Therefore, the unloading area obtained by the second optimization scheme is larger.

6. Conclusions

(1) The analytical method is used to accurately calculate the unloading area of the internal gear pump during oil trapping, and a calculation expression is given. This calculation result can be transplanted to a computer program, which can accurately simulate the trapped oil and unloading process of the internal gear pump. It has a guiding significance for the design of high-performance internal gear pumps.

(2) The calculation formula of the unloading area of the internal gear profile formed by different processing methods during oil trapping is given.

(3) The example compares the changes in the unloading area of the internal gear profile formed by the envelope method, forming tool method and die processing method during oil trapping and unloading. The larger the radius of the root circle of the internal tooth profile, the larger the unloading area, which provides a theoretical reference for the future design and improvement of the oil trapping phenomenon of the internal gear pump.

Nomenclature

z_1: Number of external gear teeth
z_2: Number of internal gear teeth
m: Modulus
e: Distance between centers of gears O_1 and O_2
α: Pressure angle
h_{a0}^*: Coefficient of rack cutter tip height
K_1: External gear profile shift coefficient
K_2: Internal gear profile shift coefficient
O_1: Center of external gear
O_2: Center of internal gear
p: Gear joint node
n_1: Meshing point
n_0: Backlash point
ud: Boundary of the rectangular unloading groove
f: Length from point p to point n_1
f_a: Length from point p to point n_1
f_b: Length from point p to point n_1
f_c: Length from point p to point n_1
f_d: Length from point p to point n_1
f_e: Length from point p to point n_1
f_f: Length from point p to point n_1
f_g: Length from point p to point n_1
p_b: Base pitch of external gear O_1
$r_{b,1}$: Base circle radius of external gear O_1
$\alpha_{a,1}$: Pressure angle of tooth top circle
α': Meshing angle
B_{ud}: Distance from ud to the line connecting O_1O_2
xOy: Coordinate system with O as origin
$x_1O_1y_1$: Coordinate system with O_1 as origin
$x_2O_2y_2$: Coordinate system with O_2 as origin
θ: Xoy rotation angle around O
θ_1: $X_1o_1y_1$ rotation angle around O_1
θ_2: $X_2o_2y_2$ rotation angle around O_2
t_1, t_2: The limit point of the involute of the gear outline
t: Sliding point from point t_1 to point t_2
t_1t_2: Contour of involute
r: Sliding point from point r_1 to point r_2
r_1,r_2: The limit point of the transition curve of gear outline
r_1r_2: Contour of transition curve
α_x: Gear pressure angle at point x
r_x: Circle radius at point x
x_x, y_x: Abscissa, ordinate in the coordinate system
θ_x: Rotation angle at point x
$\varnothing$: Angle between line t_1o_2 and t line o_2t
ζ: Angle between line r_1o_2 and t line o_2r
$s_{\text{inv}}|_{t1}^{t2}$: Area enclosed by t_1t_2, t_1o_2, and o_2t_2
$s_{\text{sta}}|_{r1}^{r2}$: Area enclosed by r_1r_2, r_1o_2, and o_2r_2
r': Pitch circle radius
$r_{a,1}$, $r_{a,2}$: Top circle of the external gear and internal gear
$r_{f,1}$, $r_{f,2}$: Root circle of the external gear and internal gear
a_1, a_2: The limit point of the addendum circle profile
c_5, c_6: The limit point of the addendum circle profile
a_5, a_6: The limit point of tooth root circle profile
c_2, c_3: The limit point of tooth root circle profile
c_1, c_4: The limit point of the transition curve of gear outline
σ: Angle between line a_1o_1 and t line o_1a_2
τ: Angle between line a_5o_1 and t line o_1a_6
μ: Angle between line c_1o_2 and t line o_2c_4
λ: Angle between line c_2o_2 and t line o_2c_3
ω: Angle between line c_5o_2 and t line o_2c_6
s_{top1}: Area enclosed by a_1a_2, a_1o_1, and o_1a_2
s_{root1}: Area enclosed by a_5a_6, a_5o_1, and o_1a_6
s_{top2}: Area enclosed by c_5c_6, c_5o_2, and o_2c_6
s_{root2}: Area enclosed by c_2c_3, c_2o_2, and o_2c_3
w: Intersection point of ud and external gear outline
v: Intersection point of ud and internal gear outline
S_1, $S_{\cap wo1n1}$: Area enclosed by o_1w, o_1n_1 and the gear outline wn_1
S_4, $S_{\cap vo2n1}$: Area enclosed by o_2v, o_2n_1 and the gear outline vn_1
S_2, $S_{\Delta o2vn1}$: Area enclosed by o_2v, o_2n_1, and vn_1
S_3, $S_{\Delta wvn1}$: Area enclosed by wv, vn_1, and wv
S_5, $S_{\Delta o1wn1}$: Area enclosed by o_1w, o_1n_1, and wn_1
S_{ud}: Unloading area
S_{uda}: Unloading area
S_{udb}: Unloading area
β_1: Angle between line po_1 and t line o_1w
γ_1: Angle between line n_1o_1 and t line o_1w
β_2: Angle between line po_2 and t line o_2v
γ_2: Angle between line n_1o_2 and t line o_2v
$r_{p,1}$: Pitch circle radius of external gear O_1
$r_{p,2}$: Pitch circle radius of internal gear O_2
$r_{n1,1}$: Meshing point radius of O_1
$r_{n1,2}$: Meshing point radius of O_2
l_{vn1}: Distances between points v and n_1
l_{wn1}: Distances between points w and n_1

l_{vw}: Distances between points v and w
r_w: Circle radius of external gear O_1 at point w
r_v: Circle radius of internal gear o_2 at point v
$\beta_{1,a1}$: Angle of β_1 when point a_1 is located on ud
$\beta_{1,a2}$: Angle of β_1 when point a_2 is located on ud
ρ_1, ρ_2, ρ_3: Half of triangle perimeter
$\beta_{2,c1}$: Angle of β_2 when point c_1 is located on ud
$\beta_{2,c4}$: Angle of β_2 when point c_4 is located on ud
$\theta_{1,a}$: Angle of θ_1 when point a is located on ud
$\theta_{1,a1}$: Angle of θ_1 when point a_1 is located on ud
$\theta_{1,a2}$: Angle of θ_1 when point a_2 is located on ud
$\theta_{1,g}$: Angle of θ_1 when point g is located on ud
$\theta_{2,a}$: Angle of θ_2 when point a is located on ud
$\theta_{2,c4}$: Angle of θ_2 when point c_4 is located on ud
$\theta_{2,c3}$: Angle of θ_2 when point c_3 is located on ud
$\theta_{2,c2}$: Angle of θ_2 when point c_2 is located on ud
$\theta_{2,c1}$: Angle of θ_2 when point c_1 is located on ud
$\theta_{2,g}$: Angle of θ_2 when point g is located on ud
r_{fa}: Root circle of internal gear
$s_{\text{root}2a}$: Area enclosed by o_2e_3, o_2e_4 and the gear outline e_3e_4
S_{1a}: Unloading area
r_{fb}: Root circle of internal gear
$s_{\text{root}2b}$: Area enclosed by o_2q_3, o_2q_4 and the gear outline q_3q_4
s_{1b}: Unloading area.

Data Availability

The data used to support the findings of this study are available from the corresponding author upon request.

Conflicts of Interest

The authors declare that there are no conflicts of interest regarding the publication of this paper.

Acknowledgments

This work was supported by Fujian Teacher Education Research Project (JAT170616) and Fujian Jiangxia College Cultivation Project (JXZ2019015).

References

[1] L. Liu and Y. Li, "Calculation and analysis of trapped oil flow in gear pumps with four different types," *Manufacturing Automation*, vol. 2, no. 37, pp. 83–85, 2015.

[2] J. Stryczek, P. Antoniak, O. Jakhno et al., "Visualisation research of the flow processes in the outlet chamber-outlet bridge-inlet chamber zone of the gear pumps," *Archives of Civil and Mechanical Engineering*, vol. 15, no. 1, pp. 95–108, 2015.

[3] N. Ertürk, A. Vernet, R. Castilla, P. J. Gamez-Montero, and J. A. Ferre, "Experimental analysis of the flow dynamics in the suction chamber of an external gear pump," *International Journal of Mechanical Sciences*, vol. 53, no. 2, pp. 135–144, 2011.

[4] F. Sun, Y. Li, and C. Wen, "Demarcated standard and verification of hacklash offload in external gear pumps," *Transactions of the Chinese Society of Agricultural Engineering*, vol. 20, no. 33, pp. 61–66, 2017.

[5] Y. Li and K. Liu, "Accurate simulation analysis of unloading area of external gear pump," *Transactions of the Chinese Society of Agricultural Engineering*, vol. 3, no. 25, pp. 42–45, 2009.

[6] K. Zang, X. Zhou, and L. Gu, "Study on new method of reducing the trap pressure of gear pump," *China Mechanical Engineering*, vol. 7, no. 15, pp. 579–582, 2004.

[7] H. Yanada, T. Ichikawa, and Y. Itsuji, "Study of the trapping of fluid in a gear pump," *Proceedings of the Institution of Mechanical Engineers Part A-Journal of Powere&.Energy*, vol. 1, no. 201, pp. 39–45, 1987.

[8] H. Zhou and W. Song, "Theoretical flow rate characteristics of the conjugated involute internal gear pump," *Proceedings of the Institution of Mechanical Engineers, Part C: Journal of Mechanical Engineering Science*, vol. 227, no. 4, pp. 730–743, 2013.

[9] W. Song, H. Zhou, and Y. G. Zhao, "Design of the conjugated straight-line internal gear pairs for fluid power gear machines," *Proceedings of the Institution of Mechanical Engineers. Part C:Journal of Mechanical Engineering Science*, vol. 8, no. 227, pp. 1776–1790, 2013.

[10] W. Song, Y. L. Chen, and H. Zhou, "Investigation of fluid delivery and trapped volume performances of Truninger gear pump by a discretization approach," *Advances in Mechanical Engineering*, vol. 10, no. 8, pp. 1–15, 2016.

[11] W. Song, *Research on Water Hydraulic Internal Gear Pump with Involute Gears*, Zhejiang University, School of Mechatronic Engineering, Zhejiang, China, 2013.

[12] C. He, *Hydraulic Components*, China Machine Press, Beijing, China, 1985.

[13] Y. Li, *Mechanism, Modeling and Experiment Investigation of Trapped Oil in External Gear Pump*, Hefei University of Technology, School of Mechanical Engineering, Hefei, China, 2009.

[14] N. D. Manring and S. B. Kasaragadda, "The theoretical flow ripple of an external gear pumps," *Transactions of the ASME*, vol. 10, no. 125, pp. 396–404, 2003.

[15] J. Zhang and L. K. Kang, "Study on hydrostatic support of inner gear in inner mesh gear pumps," *China Mechanical Engineering*, vol. 22, no. 13, pp. 1532–1537, 2011.

[16] Y. Li, F. Sun, and Y. Qi, "Light weight design of gear pumps with ultra low viscosity medium used in spacecraft," *Transactions of the Chinese Society of Agricul Tural Engineering*, vol. 32, no. 21, pp. 109–114, 2016.

[17] D. Chen, *Mechanical Design Manual*, Chemical Industry Press, Beijing, China, 2008.

[18] Y. Li and K. Liu, "Calculation of oil pumping and unloading area of gear pump with different tooth numbers," *Journal of Mechanical Transmission*, vol. 32, no. 5, pp. 53–56, 2008.